Journal of Mathematical Biology (2025) 90:36
https://doi.org/10.1007/s00285-025-02196-y

Mathematical Biology

Evaluating the long-term effects of combination antiretroviral therapy of HIV infection: a modeling study

Jing Cai[1] · Jun Zhang[2] · Kai Wang[3] · Zhixiang Dai[1] · Zhiliang Hu[4] · Yueping Dong[2] · Zhihang Peng[1,5,6]

Received: 8 July 2024 / Revised: 4 January 2025 / Accepted: 8 February 2025 /
Published online: 1 March 2025

Abstract

Current HIV/AIDS treatments effectively reduce viral loads to undetectable levels as measured by conventional clinical assays, but immune recovery remains highly variable among patients. To assess the long-term treatment efficacy, we propose a mathematical model that incorporates latently infected $CD4^+$ T cells and the homeostatic proliferation of $CD4^+$ T cells. We investigate the dynamics of this model both theoretically and numerically, demonstrating that homeostatic proliferation can induce bistability, which implies that steady-state $CD4^+$ T cell count is sensitively affected by initial conditions. The model exhibits rich dynamics, including saddle node bifurcations, Hopf bifurcations, and saddle node bifurcations related to periodic orbits. The interplay between homeostatic proliferation and latent HIV infection significantly influences the model's dynamic behavior. Additionally, we integrate combination antiretroviral therapy (cART) into the model and fit the revised model to clinical data on long-term $CD4^+$ T cell counts before and after treatment. Quantitative analysis estimates the effects of long-term cART, revealing an increasing sensitivity of steady-state $CD4^+$ T cell count to drug efficacy. Correlation analysis indicates that the heightened activation of latently infected cells helps enhance treatment efficacy. These findings underscore the critical roles of $CD4^+$ T cell homeostatic proliferation and latently infected cell production in HIV persistence despite treatment, providing valuable insights for understanding disease progression and developing more effective therapies, potentially towards eradication.

Keywords Latent HIV infection · Within-host model · Bistability · Bifurcations and periodic orbits · Data fitting

Mathematics Subject Classification 92D30 · 34D20 · 37N25

Extended author information available on the last page of the article

1 Introduction

Human immunodeficiency virus (HIV) can lead to massive reductions in $CD4^+$ T cell populations and generalized dysregulation of the immune system (Hill et al. 2018). Combination antiretroviral therapy (cART) is very effective in controlling HIV replication and preventing disease progression. With the expansion of cART, as of 2022, the AIDS-related deaths have been reduced by 69% since the peak in 2004 (UNAIDS 2023) and people in developed countries have greatly improved their health status and quality of life. However, except in rare cases, the virus is not completely eradicated from the body, resulting in a chronic state of continuous viral replication. A number of studies have been used to explain the sustained existence of viruses (Shu and Wang 2012; Reeves et al. 2018; Wang and Rong 2019; Rong et al. 2023).

The latently infected resting memory $CD4^+$ T cells are considered a major barrier to HIV eradication during cART (Chomont et al. 2009). These cells, with a median half-life of 44 months (Chun et al. 1997; Finzi et al. 1997, 1999), harbor inactivated HIV proviral DNA that persists for long periods despite treatment (Mzingwane and Tiemessen 2017). When the latently infected cells are activated, they can be induced to produce infectious viruses (Siliciano et al. 2003), which could cause viral blip or viral rebound. Besides, clinical studies have displayed that other factors, such as homeostasis of the susceptible T cell population, may also play a critical role in providing additional opportunities for HIV infection by freely moving virions (Catalfamo et al. 2011; Moreno-Fernandez et al. 2012). However, the relationship between these factors and the recovery of immune function is unclear and needs further study.

Various within-host mathematical models considering these factors aim to understand the mechanism of dynamic changes in T cell and viral load. Perelson et al. (1997) proposed an extension of a basic viral dynamic model including activation of latently infected cells to explain the second-phase decline of viral load. Kim and Perelson (2006) used a model that incorporated the rate of latently infected cell activation decreasing with time on antiretroviral therapy. Wang et al. (2017) developed a multistage latent infection model to evaluate the influence of treatment intensification with raltegravir on the viral load and 2-LTR circle dynamics. Doekes et al. (2017) employed a within-host model to explore the role of latently infected $CD4^+$ T cell reservoirs on the evolution of strains. Pankavich et al. (2020) developed a model that includes the homeostatic proliferation of $CD4^+$ T cells and shows bistability between infectious and viral clearance equilibria, along with the emergence of a Hopf bifurcation within biologically relevant parameter ranges. Moreover, some studies have explored the mechanisms underlying the persistent viral load by considering the immune response. Wang and Wang (2024) proposed a delayed HIV infection model with nonmonotonic immune response, which exhibits bistability and stable periodic solution. Wang et al. (2024) also found that the virus would rebound if the antioxidant parameter fell below the post-treatment control threshold.

There are relatively few models, including the homeostatic proliferation of $CD4^+$ T cells which are combined with clinical data in the long term (Hadjiandreou et al. 2007; Hernandez-Vargas and Middleton 2013; Loudon and Pankavich 2017). Besides, the models currently established mostly focus on either pre-cART or post-cART viral dynamics, without incorporating a combined model that integrates both states. To our

knowledge, we first attempt to propose and fit the dynamics models to the long-term CD4$^+$ T cells clinical data before and after cART, which can effectively capture the long-term trends of CD4$^+$ T cells. Our main goal is to investigate the overall cART effects on long-term trajectories of CD4$^+$ T cells and viruses.

This paper is organized as follows. In Sect. 2, we construct an HIV latent infection model considering homeostatic proliferation of CD4$^+$ T cells, and obtain the basic reproduction number $\mathcal{R}_0$. In Sect. 3, we analyze the existence and stability of equilibria of the model. In Sect. 4, the existence of forward bifurcation, backward bifurcation and Hopf bifurcation is investigated respectively. In Sect. 5, various bifurcation diagrams and solution trajectories are given to show the model dynamics and explain some biological phenomena. In Sect. 6, we introduce the cART to the model, fit it to the CD4$^+$ T cells clinical data, and perform sensitivity analysis and correlation analysis. In the last section, we provide a summary and discussion.

2 Model formulation

2.1 Mathematical model

To further study the impact of homeostatic proliferation of CD4$^+$ T cells in the context of the latent stage of infected CD4$^+$ T cells, we propose a new model including uninfected CD4$^+$ T cells $T(t)$, actively infected CD4$^+$ T cells $T_I(t)$, latently infected CD4$^+$ T cells $T_L(t)$ and viruses $V(t)$ as follows:

$$\begin{aligned}
\frac{dT(t)}{dt} &= \lambda + \frac{\rho}{\eta + V(t)} T(t)V(t) - k_1 T(t)V(t) - d_1 T(t),\\
\frac{dT_I(t)}{dt} &= \alpha k_1 T(t)V(t) + \beta T_L(t) - d_2 T_I(t),\\
\frac{dT_L(t)}{dt} &= (1-\alpha) k_1 T(t)V(t) - \beta T_L(t) - d_3 T_L(t),\\
\frac{dV(t)}{dt} &= k_2 T_I(t) - d_4 V(t)
\end{aligned} \tag{1}$$

The definitions of the model parameters are as follows. λ is the recruitment rate of uninfected CD4$^+$ T cells. The term $\frac{\rho}{\eta+V} TV$ describes the homeostatic production of CD4$^+$ T cells due to the presence of the virus and subsequent decline in uninfected CD4$^+$ T cells, where ρ is the maximum growth rate and η is the half-velocity constant of growth. k_1 represents the infection of CD4$^+$ T cells by virus. α $(0 < \alpha < 1)$ is the fraction of infected CD4$^+$ T cells become active while the rest $(1-\alpha)$ remains latent. β represents the activate rate of latently infected CD4$^+$ T cells. Free virus is produced from the actively infected CD4$^+$ T cells at the rate k_2. d_1, d_2 and d_3 are the death rates of uninfected CD4$^+$ T cells, actively infected CD4$^+$ T cells and latently infected CD4$^+$ T cells, respectively. d_4 is the clearance rate of free virus particles. All parameters are positive constants (see Table 1 in detail).

2.2 Positivity of solutions

To show that model (1) is biologically meaningful, it is essential to disclose that all the state variables are non-negative for all time $t > 0$. For this purpose, we have the following results.

Lemma 2.1 *Every solution of model* (1) *with positive initial conditions remains positive in* $\mathbb{R}_4^+$ *as* $t > 0$.

Proof From model (1), it is easy to obtain

$$\begin{aligned}
\frac{dT}{dt} &= \Big|_{[T=0,T_I\geq 0,T_L\geq 0,V\geq 0]} = \lambda > 0,\\
\frac{dT_I}{dt} &= \Big|_{[T\geq 0,T_I=0,T_L\geq 0,V\geq 0]} = \alpha k_1 TV + \beta T_L \geq 0,\\
\frac{dT_L}{dt} &= \Big|_{[T\geq 0,T_I\geq 0,T_L=0,V\geq 0]} = (1-\alpha)k_1 TV \geq 0,\\
\frac{dV}{dt} &= \Big|_{[T\geq 0,T_I\geq 0,T_L\geq 0,V=0]} = k_2 T_I \geq 0.
\end{aligned}$$

The above rates are all non-negative over the boundary planes of the non-negative cone of $\mathbb{R}_4$ (Perelson et al. 1993; Zhang et al. 2024). Therefore, all the solutions with positive initial conditions will remain in the positive region only. □

2.3 Basic reproduction number

Obviously, the infection-free equilibrium of model (1) is $E_0 = (\frac{\lambda}{d_1}, 0, 0, 0)$. We use the next generation matrix method (Van den Driessche and Watmough 2002) to obtain the basic reproduction number $\mathcal{R}_0$. Let us consider $X = (T_I, T_L, V)$, and model (1) is written as $\dot{X} = \mathcal{F} - \mathcal{V}$, where

$$\mathcal{F} = \begin{pmatrix} \alpha k_1 TV \\ (1-\alpha)k_1 TV \\ 0 \end{pmatrix}, \quad \mathcal{V} = \begin{pmatrix} -\beta T_L + d_2 T_I \\ \beta T_L + d_3 T_L \\ -k_2 T_I + d_4 V \end{pmatrix}.$$

Jacobian matrices $\mathbb{F}$ and $\mathbb{V}$ at $E_0 = (\frac{\lambda}{d_1}, 0, 0, 0)$ of $\mathcal{F}$ and $\mathcal{V}$ are given by

$$\mathbb{F} = \begin{pmatrix} 0 & 0 & \frac{\alpha k_1 \lambda}{d_1} \\ 0 & 0 & \frac{k_1\lambda(1-\alpha)}{d_1} \\ 0 & 0 & 0 \end{pmatrix}, \quad \mathbb{V} = \begin{pmatrix} d_2 & -\beta & 0 \\ 0 & \beta + d_3 & 0 \\ -k_2 & 0 & d_4 \end{pmatrix}.$$

Then the next generation matrix is

$$\mathbb{FV}^{-1} = \begin{pmatrix} \frac{\alpha k_1 k_2 \lambda}{d_1 d_2 d_4} & \frac{\alpha\beta k_1 k_2 \lambda}{d_1 d_2 d_4(\beta+d_3)} & \frac{\alpha k_1 \lambda}{d_1 d_4} \\ \frac{k_1 k_2 \lambda(1-\alpha)}{d_1 d_2 d_4} & \frac{\beta k_1 k_2 \lambda(1-\alpha)}{d_1 d_2 d_4(\beta+d_3)} & \frac{k_1 \lambda(1-\alpha)}{d_1 d_4} \\ 0 & 0 & 0 \end{pmatrix}.$$

The basic reproduction number $\mathcal{R}_0$ is the spectral radius of $\mathbb{FV}^{-1}$, that is,

$$\mathcal{R}_0 = \frac{k_1 k_2 \lambda(\beta + \alpha d_3)}{d_1 d_2 d_4(\beta + d_3)}.$$

3 Existence and stability of equilibria

3.1 Existence of equilibria

To find the equilibria of model (1), we set

$$\begin{cases} \lambda + \dfrac{\rho}{\eta + V} T V - k_1 T V - d_1 T = 0, \\ \alpha k_1 T V + \beta T_L - d_2 T_I = 0, \\ (1-\alpha) k_1 T V - \beta T_L - d_3 T_L = 0, \\ k_2 T_I - d_4 V = 0. \end{cases} \tag{2}$$

When $V = 0$, it is easy to get that $T^0 = \frac{\lambda}{d_1}$ and $T_I^0 = T_L^0 = 0$, that is, the infection-free equilibrium $E_0(\frac{\lambda}{d_1}, 0, 0, 0)$ always exists.

If the infected equilibrium $E^*(T^*, T_I^*, T_L^*, V^*)$ exists, then all components T^*, T_I^*, T_L^*, V^* should satisfy the equation (2) and be positive. When $V^* > 0$, from the last three equations of (2), by calculations, T^*, T_I^* and T_L^* can be represented by V^*, that is,

$$T^* = \frac{d_2 d_4 (\beta + d_3)}{k_1 k_2 (\beta + \alpha d_3)}, \ T_I^* = \frac{d_4}{k_2} V^*, \ T_L^* = \frac{d_2 d_4 (1-\alpha)}{k_2 (\beta + \alpha d_3)} V^*. \tag{3}$$

Note that the expression of T^* is only related to some parameters and is irrelevant to V^*. Next, substituting (3) into the first equation of (2) gives

$$\frac{A_1 V^{*2} + A_2 V^* + A_3}{k_1 k_2 (\beta + \alpha d_3) V^* + \eta k_1 k_2 (\beta + \alpha d_3)} = 0, \tag{4}$$

where

$$\begin{aligned} A_1 &= -d_2 d_4 k_1 (\beta + d_3) < 0, \\ A_2 &= k_1 k_2 \lambda (\beta + \alpha d_3) - d_1 d_2 d_4 (\beta + d_3) + d_2 d_4 (\beta + d_3)(\rho - \eta k_1) \\ &= d_2 d_4 (\beta + d_3)[d_1 (\mathcal{R}_0 - 1) + (\rho - \eta k_1)], \\ A_3 &= \eta [k_1 k_2 \lambda (\beta + \alpha d_3) - d_1 d_2 d_4 (\beta + d_3)] \\ &= \eta d_1 d_2 d_4 (\beta + d_3)(\mathcal{R}_0 - 1). \end{aligned}$$

Notice that all parameters are greater than 0 and V^* is non-negative. Therefore, the product of the parameters and V^*, along with the product of the parameters themselves, is greater than 0. As a result, the denominator of (4) is always positive and $A_1 < 0$. Define $f(V^*) = A_1 (V^*)^2 + A_2 V^* + A_3$ and $\Delta = A_2^2 - 4A_1 A_3$, where $f(V^*)$ is a parabola function that opens downward. So next we discuss the number of positive roots of $f(V^*) = 0$ for the following cases.

Case 1: $A_3 < 0$, corresponding to $\mathcal{R}_0 < 1$:

- when $A_2 \leqslant 0$, $f(V^*) = 0$ has no positive root;
- when $A_2 > 0$, $f(V^*) = 0$ has two positive roots $V_1^* = \frac{-A_2 + \sqrt{\Delta}}{2A_1}$ and $V_2^* = \frac{-A_2 - \sqrt{\Delta}}{2A_1}$ if $\Delta > 0$; $f(V^*) = 0$ has one positive root $V_1^* = -\frac{A_2}{2A_1}$ if $\Delta = 0$; and $f(V^*) = 0$ has no positive root if $\Delta < 0$.

Case 2: $A_3 = 0$, corresponding to $\mathcal{R}_0 = 1$:

- when $A_2 \leqslant 0$, $f(V^*) = 0$ has no positive root;
- when $A_2 > 0$, $f(V^*) = 0$ has one positive root $V_1^* = -\frac{A_2}{A_1}$.

Case 3: $A_3 > 0$, corresponding to $\mathcal{R}_0 > 1$:

- $f(V^*) = 0$ always has one positive root $V_1^* = \frac{-A_2 + \sqrt{\Delta}}{2A_1}$.

To sum up, we have the following proposition for the existence of equilibria of model (1).

Proposition 3.1 *The infection-free equilibrium* $E_0(\frac{\lambda}{d_1}, 0, 0, 0)$ *of model* (1) *always exists, and the model has at most two infected equilibria* E_1^* *(higher viral load) and* E_2^* *(lower viral load). Moreover,*

- *if* $\mathcal{R}_0 = 1$, *model* (1) *has one infected equilibrium* E_1^* *when* $A_2 > 0$*;*
- *if* $\mathcal{R}_0 > 1$, *model* (1) *always has one infected equilibrium* E_1^**;*
- *if* $\mathcal{R}_0 < 1$, *model* (1) *has one infected equilibrium* E_1^* *when* $A_2 > 0$ *and* $\Delta = 0$*; model* (1) *has two infected equilibria* E_1^* *and* E_2^* *when* $A_2 > 0$ *and* $\Delta > 0$*,*
- *In other cases, model* (1) *does not have infected equilibrium.*

3.2 Stability of infection-free equilibrium

Theorem 3.1 *The infection-free equilibrium* E_0 *of model (1) is locally asymptotically stable if* $\mathcal{R}_0 < 1$, *and unstable if* $\mathcal{R}_0 > 1$.

Proof The Jacobian matrix of model (1) at equilibrium $E_0 = (\frac{\lambda}{d_1}, 0, 0, 0)$ is

$$J_{E_0} = \begin{pmatrix} -d_1 & 0 & 0 & \frac{\lambda(\rho - k_1\eta)}{d_1\eta} \\ 0 & -d_2 & \beta & \frac{\alpha k_1 \lambda}{d_1} \\ 0 & 0 & -\beta - d_3 & \frac{k_1\lambda(1-\alpha)}{d_1} \\ 0 & k_2 & 0 & -d_4 \end{pmatrix}.$$

Obviously, $-d_1$ is a negative eigenvalue of matrix J_{E_0}.

For the submatrix

$$J = \begin{pmatrix} -d_2 & \beta & \frac{\alpha k_1 \lambda}{d_1} \\ 0 & -\beta - d_3 & \frac{k_1\lambda(1-\alpha)}{d_1} \\ k_2 & 0 & -d_4 \end{pmatrix},$$

the corresponding characteristic equation is

$$r^3 + a_1 r^2 + a_2 r + a_3 = 0,$$

where

$$\begin{aligned} a_1 &= \beta + d_2 + d_3 + d_4, \\ a_2 &= \frac{\beta d_1 d_2 + \beta d_1 d_4 + d_1 d_2 d_3 + d_1 d_2 d_4 + d_1 d_3 d_4 - \alpha k_1 k_2 \lambda}{d_1}, \\ a_3 &= \frac{d_1 d_2 d_4 (\beta + d_3) - k_1 k_2 \lambda (\beta + \alpha d_3)}{d_1} = d_2 d_4 (\beta + d_3)(1 - \mathcal{R}_0). \end{aligned}$$

It is easy to observe that $H_1 = a_1 > 0$ and the sign of a_3 is determined by the size of $\mathcal{R}_0$. By calculations, we have

$$\begin{aligned} H_2 = a_1 a_2 - a_3 &= \frac{1}{d_1}[(\beta + d_2 + d_3 + d_4) \\ &\quad (\beta d_1 d_2 + \beta d_1 d_4 + d_1 d_2 d_3 + d_1 d_2 d_4 + d_1 d_3 d_4 - \alpha k_1 k_2 \lambda) \\ &\quad + \beta k_1 k_2 \lambda - \beta d_1 d_2 d_4 - d_1 d_2 d_3 d_4 + \alpha d_3 k_1 k_2 \lambda] \\ &= \frac{1}{d_1}[(\beta + d_2 + d_3 + d_4)(d_1 d_2 d_4 - \alpha k_1 k_2 \lambda) \\ &\quad + (\beta + d_2 + d_3 + d_4)(\beta d_1 d_2 + \beta d_1 d_4 + d_1 d_2 d_3 + d_1 d_3 d_4) \\ &\quad + \beta k_1 k_2 \lambda - \beta d_1 d_2 d_4 - d_1 d_2 d_3 d_4 + \alpha d_3 k_1 k_2 \lambda] \\ &= \frac{1}{d_1}[(\beta + d_2 + d_3 + d_4)(d_1 d_2 d_4 - \alpha k_1 k_2 \lambda) \\ &\quad + (\beta + d_2 + d_3)(\beta d_1 d_2 + \beta d_1 d_4 + d_1 d_2 d_3 + d_1 d_3 d_4) \\ &\quad + d_4(\beta d_1 d_4 + d_1 d_3 d_4) + \beta k_1 k_2 \lambda + \alpha d_3 k_1 k_2 \lambda]. \end{aligned}$$

Since

$$\mathcal{R}_0 = \frac{k_1 k_2 \lambda\,(\beta + \alpha d_3)}{d_1 d_2 d_4\,(\beta + d_3)} < 1 \Longleftrightarrow k_1 k_2 \lambda < \frac{d_1 d_2 d_4\,(\beta + d_3)}{(\beta + \alpha d_3)},$$

we have

$$\begin{aligned} d_1 d_2 d_4 - \alpha k_1 k_2 \lambda &> d_1 d_2 d_4 - \alpha \frac{d_1 d_2 d_4\,(\beta + d_3)}{(\beta + \alpha d_3)} \\ &= \frac{d_1 d_2 d_4\,(\beta + \alpha d_3) - \alpha d_1 d_2 d_4\,(\beta + d_3)}{(\beta + \alpha d_3)} \\ &= \frac{(1-\alpha)\,\beta d_1 d_2 d_4}{(\beta + \alpha d_3)} > 0. \end{aligned}$$

Therefore, $d_1 d_2 d_4 - \alpha k_1 k_2 \lambda > 0$ if $\mathcal{R}_0 < 1$, which implies that $H_2 > 0$ if $\mathcal{R}_0 < 1$.

By the well-known Routh–Hurwitz criterion (DeJesus and Kaufman 1987), it is obtained that the real parts of all eigenvalues of the submatrix J are negative if $\mathcal{R}_0 < 1$, and the real parts of all eigenvalues of J have at least one positive root if $\mathcal{R}_0 > 1$. Hence the above result is obtained. □

3.3 Stability of infected equilibria

Theorem 3.2 *The infected equilibrium E^* of model (1) is locally asymptotically stable provided that*

$$b_1 b_2 b_3 - b_3^2 - b_1^2 b_4 > 0$$

holds true, where b_i $(i = 1, 2, 3, 4)$ are given by (6).

Proof The Jacobian matrix of model (1) at any infected equilibrium $E^* = (T^*, T_I^*, T_L^*, V^*)$ is

$$\begin{aligned} J_{E^*} &= \begin{pmatrix} \frac{\rho V^*}{V^*+\eta} - k_1 V^* - d_1 & 0 & 0 & \frac{\rho\eta T^*}{(V^*+\eta)^2} - k_1 T^* \\ \alpha k_1 V^* & -d_2 & \beta & \alpha k_1 T^* \\ k_1\,(1-\alpha)\,V^* & 0 & -\beta - d_3 & k_1\,(1-\alpha)\,T^* \\ 0 & k_2 & 0 & -d_4 \end{pmatrix} \\ &= \begin{pmatrix} -\frac{\lambda}{T^*} & 0 & 0 & N \\ \alpha k_1 V^* & -d_2 & \beta & \alpha k_1 T^* \\ k_1\,(1-\alpha)\,V^* & 0 & -\beta - d_3 & k_1\,(1-\alpha)\,T^* \\ 0 & k_2 & 0 & -d_4 \end{pmatrix}, \end{aligned}$$

where $N = \frac{\rho\eta T^*}{(V^*+\eta)^2} - k_1 T^*$ and $\frac{\rho V^*}{V^*+\eta} - k_1 V^* - d_1 = -\frac{\lambda}{T^*}$.

Firstly, we prove that N is always negative for any $V^* > 0$. It is easy to obtain that

$$\frac{\rho V^*}{V^* + \eta} - k_1 V^* - d_1 < 0 \text{ for any } V^* > 0,$$

which is equivalent to

$$V^* + \eta > \frac{\rho V^*}{k_1 V^* + d_1} \text{ for any } V^* > 0.$$

The arbitrariness of V^* implies that

$$V^* + \eta > \max\left\{\frac{\rho V^*}{k_1 V^* + d_1}\right\},$$

that is $V^* + \eta > \frac{\rho}{k_1}$. Furthermore, we have

$$\left(V^* + \eta\right)^2 > \frac{\rho}{k_1}\left(V^* + \eta\right) > \frac{\rho\eta}{k_1},$$

which is equivalent to

$$\frac{\rho\eta}{(V^* + \eta)^2} < k_1.$$

Therefore, we conclude that $N < 0$.

Next, by calculations, the corresponding characteristic equation of the matrix J_{E^*} is given by

$$r^4 + b_1 r^3 + b_2 r^2 + b_3 r + b_4 = 0, \tag{5}$$

where

$$\begin{aligned}
b_1 &= \frac{\lambda}{T^*} + \beta + d_2 + d_3 + d_4,\\
b_2 &= \frac{\lambda\left(\beta + d_2 + d_3 + d_4\right)}{T^*} + \beta d_2 + \beta d_4 + d_2 d_3 + d_2 d_4 + d_3 d_4 - \alpha k_1 k_2 T^*,\\
b_3 &= \frac{\lambda\left(\beta d_2 + \beta d_4 + d_2 d_3 + d_2 d_4 + d_3 d_4 - \alpha k_1 k_2 T^*\right)}{T^*}\\
&\quad + d_2 d_4\left(\beta + d_3\right) - k_1 k_2 T^*\left(\beta + \alpha d_3\right) - \alpha k_1 k_2 N V^* T^*,\\
b_4 &= \frac{\lambda\left[d_2 d_4\left(\beta + d_3\right) - k_1 k_2 T^*\left(\beta + \alpha d_3\right)\right]}{T^*} - k_1 k_2 N V^*\left(\beta + \alpha d_3\right).
\end{aligned} \tag{6}$$

From (3), we conclude that

$$d_2 d_4\left(\beta + d_3\right) - k_1 k_2 T^*\left(\beta + \alpha d_3\right) = 0$$

and

$$d_2d_4 - \alpha k_1k_2T^* = d_2d_4 - \alpha k_1k_2 \cdot \frac{d_2d_4\,(\beta + d_3)}{k_1k_2\,(\beta + \alpha d_3)} = \frac{\beta d_2d_4\,(1-\alpha)}{(\beta + \alpha d_3)} > 0,$$

which implies that $b_i > 0$ for $i = 1, 2, 3, 4$.

The well-known Routh–Hurwitz criterion (DeJesus and Kaufman 1987) shows that the real part of all characteristic roots of matrix J_{E^*} is negative if and only if

$$L_1 = b_1 > 0,\ L_2 = b_1b_2 - b_3 > 0,\ L_3 = b_1b_2b_3 - b_3^2 - b_1^2b_4 > 0 \text{ and } L_4 = L_3b_4 > 0.$$

Since $L_3 = b_3L_2 - b_1^2b_4$, it is easy to see that if L_3 is greater than 0, then L_2 is greater than 0. And if L_2 is less than 0, L_3 must be less than 0. Hence the stability of the infected equilibrium E^* of model (1) is determined by $L_3 = b_1b_2b_3 - b_3^2 - b_1^2b_4$. □

4 Bifurcation analysis

4.1 Forward and backward bifurcations at infection-free equilibrium

Lemma 4.1 (see Theorem 4.1 in Castillo-Chavez and Song 2004) *Consider a general system of ODEs with a parameter ϕ:*

$$\frac{dx}{dt} = f(x, \phi), \quad f : \mathbb{R}^n \times \mathbb{R} \to \mathbb{R}^n \text{ and } f \in \mathbb{C}^2\left(\mathbb{R}^n \times \mathbb{R}\right). \tag{7}$$

Without loss of generality, it is assumed that $\boldsymbol{0}$ is an equilibrium for system (7) for all values of the parameter ϕ, that is

$$f(\boldsymbol{0}, \phi) \equiv \boldsymbol{0} \text{ for all } \phi.$$

Furthermore, assume

1. *$A = D_x f(\boldsymbol{0}, 0) = \left(\frac{\partial f_i}{\partial x_j}(\boldsymbol{0}, 0)\right)$ is the linearization matrix of system (7) around the equilibrium $\boldsymbol{0}$ with ϕ evaluated at 0. Zero is a simple eigenvalue of A and all other eigenvalues of A have negative real parts.*
2. *Matrix A has a nonnegative right eigenvector w and a left eigenvector v corresponding to the zero eigenvalue.*

Let f_k be the k-th component of f and

$$a = \sum_{k,i,j=1}^{n} v_k w_i w_j \frac{\partial^2 f_k}{\partial x_i \partial x_j}(\boldsymbol{0}, 0),$$

$$b = \sum_{k,i=1}^{n} v_k w_i \frac{\partial^2 f_k}{\partial x_i \partial \phi}(\boldsymbol{0}, 0).$$

The local dynamics of (7) *around equilibrium* $\boldsymbol{0}$ *are totally determined by a and b as follows:*

1. $a > 0, b > 0$. *When* $\phi < 0$ *with* $|\phi| \ll 1$, *equilibrium* $\boldsymbol{0}$ *is locally asymptotically stable, and there exists an unstable infected equilibrium; when* $0 < \phi \ll 1$, $\boldsymbol{0}$ *is unstable and there exists a negative and locally asymptotically stable equilibrium, which corresponds to the forward bifurcation at* $\phi = 0$ *for equilibrium* $\boldsymbol{0}$.
2. $a < 0, b > 0$. *When* ϕ *changes from negative to positive, equilibrium* $\boldsymbol{0}$ *changes its stability from stable to unstable and a negative unstable equilibrium becomes positive and locally asymptotically stable, which corresponds to the backward bifurcation at* $\phi = 0$ *for equilibrium* $\boldsymbol{0}$.

Remark 1 (see Remark 1 in Castillo-Chavez and Song 2004) The requirement that w is nonnegative is not necessary; that is, $w(j) > 0$ whenever $\mathbf{x}(j) = 0$, and $w(j)$ does not need to be positive if $\mathbf{x}(j) > 0$, where $\mathbf{x}(j)$ is the j-th component of the nonnegative equilibrium $\mathbf{x}$ of system (7).

To apply this method in our model (1), we first denote the system with defining by $T = x_1, T_I = x_2, T_L = x_3, V = x_4$ and rewrite the model (1) as follows:

$$\begin{aligned}
\frac{dx_1}{dt} &= \lambda + \frac{\rho}{\eta + x_4} x_1 x_4 - k_1 x_1 x_4 - d_1 x_1 \triangleq f_1, \\
\frac{dx_2}{dt} &= \alpha k_1 x_1 x_4 + \beta x_3 - d_2 x_2 \triangleq f_2, \\
\frac{dx_3}{dt} &= (1-\alpha) k_1 x_1 x_4 - \beta x_3 - d_3 x_3 \triangleq f_3, \\
\frac{dx_4}{dt} &= k_2 x_2 - d_4 x_4 \triangleq f_4.
\end{aligned} \tag{8}$$

Next we investigate the direction of the bifurcation around infection-free equilibrium $E_0 = \left(x_1^*, x_2^*, x_3^*, x_4^*\right)$ where $x_1^* = \frac{\lambda}{d_1}$ and $x_2^* = x_3^* = x_4^* = 0$. We know that $\mathcal{R}_0$ (α is proportional to $\mathcal{R}_0$) determines the local stability of E_0, that is, it determines the sign of real part of a characteristic root of J_{E_0} (other characteristic roots have negative real parts). Therefore, we choose parameter α as the bifurcation parameter, where $\alpha^* = \frac{d_1 d_2 d_4 (\beta + d_3) - \beta k_1 k_2 \lambda}{d_3 k_1 k_3 \lambda}$ by direct computation from $\mathcal{R}_0 = 1$. When $\alpha = \alpha^*$, the Jacobian matrix of model (8) at equilibrium E_0 is

$$J_{E_0}\left(\alpha^*\right) = \begin{pmatrix} -d_1 & 0 & 0 & \frac{\lambda(\rho - k_1\eta)}{d_1 \eta} \\ 0 & -d_2 & \beta & \frac{k_1 \lambda \alpha^*}{d_1} \\ 0 & 0 & -\beta - d_3 & \frac{k_1 \lambda (1-\alpha^*)}{d_1} \\ 0 & k_2 & 0 & -d_4 \end{pmatrix}.$$

The associated right and left eigenvectors corresponding to the zero eigenvalue are $w = (w_1, w_2, w_3, w_4)^T$ and $v = (v_1, v_2, v_3, v_4)$ respectively, where

$$w_1 = \frac{k_2\lambda(\rho - \eta k_1)}{d_1^2 d_4 \eta} w_2,\ w_3 = \frac{k_1 k_2 \lambda(1-\alpha)}{d_1 d_4(\beta + d_3)} w_2,$$
$$w_4 = \frac{k_2}{d_4} w_2,\ w_2 > 0 \text{ is free},$$

and

$$v_1 = 0,\ v_3 = \frac{\beta}{\beta + d_3} v_2,\ v_4 = \frac{d_2}{k_2} v_2,\ v_2 > 0 \text{ is free}.$$

Clearly, $v_i \geqslant 0$ and $w_i \geqslant 0$ when $2 \leqslant i \leqslant 4$. By applying Remark 1, the requirement that w_1 is nonnegative is not necessary. Algebraic calculations show that

$$\begin{aligned} a &= 2v_2 w_1 w_4 \frac{\partial^2 f_2}{\partial x_1 \partial x_4}\left(E_0, \alpha^*\right) + 2v_3 w_1 w_4 \frac{\partial^2 f_3}{\partial x_1 \partial x_4}\left(E_0, \alpha^*\right) \\ &= 2v_2 w_1 w_4 \cdot k_1 \alpha^* + 2v_3 w_1 w_4 \cdot k_1\left(1 - \alpha^*\right) \\ &= 2w_1 w_4 k_1\left[\alpha^* v_2 + \left(1 - \alpha^*\right) v_3\right] \end{aligned}$$

and

$$\begin{aligned} b =& 2v_2\left(w_1 \cdot \frac{\partial^2 f_2}{\partial x_1 \partial \alpha}\left(E_0, \alpha^*\right) + w_4 \cdot \frac{\partial^2 f_2}{\partial x_4 \partial \alpha}\left(E_0, \alpha^*\right)\right) \\ &+ 2v_3\left(w_1 \cdot \frac{\partial^2 f_3}{\partial x_1 \partial \alpha}\left(E_0, \alpha^*\right) + w_4 \cdot \frac{\partial^2 f_3}{\partial x_4 \partial \alpha}\left(E_0, \alpha^*\right)\right) \\ =& 2v_2\left(w_1 \cdot k_1 x_4^* + w_4 \cdot k_1 x_1^*\right) + 2v_3\left(-w_1 \cdot k_1 x_4^* - w_4 \cdot k_1 x_1^*\right) \\ =& 2w_4 k_1 x_1^*\left(v_2 - v_3\right) \\ =& \frac{2k_1\lambda d_3}{d_1(\beta + d_3)} w_4 v_2 > 0. \end{aligned}$$

It is easy to see that the sign of a is determined by w_1, that is,

$$\operatorname{sign}[a] = \operatorname{sign}[w_1] = \operatorname{sign}[\rho - \eta k_1].$$

Therefore, we have $a > 0$ when $\rho > \overline{\rho} \triangleq \eta k_1$, and obtain the following result for the direction of the bifurcation around infection-free equilibrium E_0.

Theorem 4.2 *If $\rho < \overline{\rho}$, a forward bifurcation around infection-free equilibrium E_0 of model (1) occurs at $\alpha = \alpha^*$, corresponding to $\mathcal{R}_0 = 1$, and the direction of the bifurcation is backward if $\rho > \overline{\rho}$.*

Remark 2 Theorem 4.2 demonstrates that a large value of parameter ρ leads to backward bifurcation in the model, potentially resulting in bistability of E_0 and E_1^*.

Biologically, the mechanism of homeostatic proliferation of $CD4^+$ T cells makes whether HIV infection can be cleared greatly depend on the initial conditions, which may be the potential reason why the HIV treatment scenario is so complicated.

4.2 Local Hopf bifurcation at infected equilibrium

In this subsection, we explore the existence of Hopf bifurcation at infected equilibrium $E^* = (T^*, T_I^*, T_L^*, V^*)$ when parameter ρ is used as the bifurcation parameter. Assume that $\lambda = i\omega$, where $\omega \in \mathbb{R}^+$ is the root of the characteristic equation (5). Substituting it into (5) yields

$$\omega^4 - b_1\omega^3 i - b_2\omega^2 + b_3\omega i + b_4 = 0.$$

Separating the real and imaginary parts, we have

$$\begin{cases} \omega^4 - b_2\omega^2 + b_4 = 0, \\ -b_1\omega^3 + b_3\omega = 0, \end{cases}$$

which is equivalent to

$$\begin{cases} b_3^2 + b_1^2 b_4 - b_1 b_2 b_3 = 0, \\ \omega^2 = \frac{b_3}{b_1}. \end{cases}$$

Denote $\Theta(\rho) = b_3^2 + b_1^2 b_4 - b_1 b_2 b_3 = 0$. Then both $\Theta(\rho)$ and $b_i (i = 1, 2, 3, 4)$ are functions of ρ. Obviously, a pair of pure imaginary roots $\lambda = \pm i\omega$ of the characteristic equation exists only if there exists $\rho > 0$ such that $\Theta(\rho) = 0$. Suppose that $\Theta(\rho) = 0$ has at least one positive real root ρ^*. Next, we validate the transversality condition of Hopf bifurcation.

By differentiating $P(\lambda; \rho) = 0$ defined in (5) with respect to ρ, we have

$$\frac{d\lambda}{d\rho} = -\frac{b_1'\lambda^3 + b_2'\lambda^2 + b_3'\lambda + b_4'}{4\lambda^3 + 3b_1\lambda^2 + 2b_2\lambda + b_3},$$

where b_i' is the derivative of b_i with respect to ρ. Furthermore, $P(i\omega; \rho^*) = 0$ implies that

$$\left.\frac{d\lambda}{d\rho}\right|_{\lambda=i\omega} = -\frac{-b_1'\omega^3 i - b_2'\omega^2 + b_3'\omega i + b_4'}{-4\omega^3 i - 3b_1\omega^2 + 2b_2\omega i + b_3} = -\frac{b_4' - b_2'\omega^2 + \left(b_3'\omega - b_1'\omega^3\right) i}{b_3 - 3b_1\omega^2 + \left(2b_2\omega - 4\omega^3\right) i}.$$

By calculations, we have

$$\begin{aligned}\mathrm{Re}\left(\frac{d\lambda}{d\rho}\Big|_{\lambda=i\omega}\right) &= -\frac{\left[\left(b_4' - b_2'\omega^2\right)\left(b_3 - 3b_1\omega^2\right) + \left(b_3'\omega - b_1'\omega^3\right)\left(2b_2\omega - 4\omega^3\right)\right]}{\left(b_3 - 3b_1\omega^2\right)^2 + \left(2b_2\omega - 4\omega^3\right)^2} \\ &= \frac{b_1\Theta'(\rho^*)}{2\left[(b_1b_2 - 2b_3)^2 + b_1^3b_3\right]},\end{aligned}$$

where

$$\Theta'(\rho) = b_1'(2b_1b_4 - b_2b_3) - b_2'b_1b_3 + b_3'(2b_3 - b_1b_2) + b_4'b_1^2.$$

Therefore, we obtain that

$$\mathrm{sign}\left[\frac{d\lambda}{d\rho}\Big|_{\lambda=i\omega}\right] = \mathrm{sign}\left[\frac{d\Theta(\rho)}{d\rho}\Big|_{\rho=\rho^*}\right].$$

Based on the above discussion, we have the following result by applying the Hopf bifurcation theorem (Marsden and McCracken 1976).

Theorem 4.3 *If there exists* $\rho^* > 0$ *such that* $\Theta(\rho^*) = 0$ *and* $\frac{d\Theta(\rho)}{d\rho}\Big|_{\rho=\rho^*} \neq 0$, *then model* (1) *undergoes a Hopf bifurcation at infected equilibrium* $E^* = (T^*, T_I^*, T_L^*, V^*)$ *when* $\rho = \rho^*$.

5 Rich dynamics of model (1)

In this section, we draw some bifurcation diagrams and solution trajectories by using MATCONT (Dhooge et al. 2003) in MATLAB to illustrate the rich and interesting dynamics. Parameter values not specifically stated are from Table 1.

Figure 1 shows the dynamic behaviors of model (1) in (ρ, α) plane, which is divided into six regions by the line $\alpha = \alpha^* = 0.3179$ (orange line), saddle node bifurcation curve (green curve) and two Hopf bifurcation curves (magenta curves). When the values of parameters ρ and α cross the saddle node bifurcation curve from region ③ to ④ or ⑤, two infected equilibria E_1^* (higher virus load) and E_2^* (lower virus load) appear. Besides, model (1) undergoes a Hopf bifurcation when ρ and α cross the Hopf bifurcation curve. And Hopf bifurcation is supercritical when it crosses the solid magenta curve where a stable periodic orbit is produced, while it is subcritical when it passes through the dashed magenta curve where an unstable periodic orbit is appeared. The existence and corresponding local stability of equilibrium points of model (1) in each region of Fig. 1 are summarized in Table 2.

Furthermore, in Fig. 1, $\rho = 1,\ 1.3,\ 1.4,\ 1.8,\ 2$ and 3.9 are fixed and then we draw the corresponding bifurcation diagrams of component V of equilibria of model (1) with respect to parameter α, which is depicted in Fig. 2. Notation SN represents the saddle node bifurcation point and H expresses Hopf bifurcation point where the

Table 1 Definition of the parameters and their values

Parameter and its description		Value	Source
λ	Recruitment rate of uninfected $CD4^+$ T cells	$10\,mm^{-3}day^{-1}$	Perelson et al. (1993)
ρ	Maximum growth rate	$0.01\ day^{-1}$	Pankavich et al. (2020)
η	Half-velocity constant of growth	300 copies mm^{-3}	Pankavich et al. (2020)
k_1	Infection rate of uninfected $CD4^+$ T cells by virus	$0.00387\ mm^3day^{-1}$	Hadjiandreou et al. (2007)
α	Fraction of infected $CD4^+$ T cells become active	0.97	Hadjiandreou et al. (2007)
β	Activate rate of latently infected $CD4^+$ T cells	$0.0003\ day^{-1}$	Dong and Ma (2012)
k_2	Production rate of virus	$0.537\ mm^3day^{-1}$	Dong and Ma (2012)
d_1	Death rate of uninfected $CD4^+$ T cells	$0.01\ day^{-1}$	Dong and Ma (2012)
d_2	Death rate of actively infected $CD4^+$ T cells	$0.28\ day^{-1}$	Dong and Ma (2012)
d_3	Death rate of latently infected $CD4^+$ T cells	$0.05\ day^{-1}$	Dong and Ma (2012)
d_4	Clearance rate of free virus particles	$2.39\ day^{-1}$	Dong and Ma (2012)

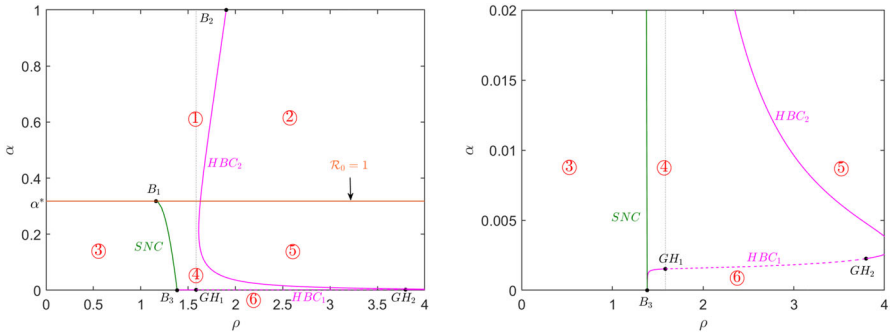

(a) (b) The local enlarged view of (a)

Fig. 1 Saddle node bifurcation curve (green curve and marked SNC) and Hopf bifurcation curves (magenta curves and marked HBC_i, $i = 1, 2$) in (ρ, α) plane, where the solid (dashed) magenta line represents the supercritical (subcritical) Hopf bifurcation. The orange line represents $\alpha = \alpha^* = 0.3179$ corresponding to $\mathcal{R}_0 = 1$. The thresholds $B_1 = (1.161, 0.3179)$, $B_2 = (1.903, 1)$, $B_3 = (1.384, 0)$ are critical points and $GH_1 = (1.584, 0.001523)$, $GH_2 = (3.797, 0.002257)$ are Generalized Hopf (Bautin) bifurcation points. All other parameter values except parameters ρ and α are taken from Table 1

Table 2 The existence and corresponding local stability of equilibrium points of model (1) in Fig. 1

Region	Stability	
①	E_0 (unstable)	E_1^* (stable)
②	E_0 (unstable)	E_1^* (unstable)
③	E_0 (stable)	–
④	E_0 (stable)	E_1^* (stable) and E_2^* (unstable)
⑤	E_0 (stable)	E_1^* (unstable) and E_2^* (unstable)
⑥	E_0 (stable)	E_1^* (unstable) and E_2^* (unstable)

subscripts $super$ and sub represent that the Hopf bifurcation is supercritical and subcritical, respectively. Figure 2a, b show the classic forward and backward bifurcations. Figure 2c shows a supercritical Hopf bifurcation point H_{super} on the larger infected equilibrium E_1^*. Figure 2d shows three Hopf bifurcation points H_{sub}, $\bar{H}_{super}$ and $\bar{\bar{H}}_{super}$. Figure 2e, f show two Hopf bifurcation points. The corresponding thresholds of all special points regarding parameter α are shown in Table 3.

By calculations, $\bar{\rho} = \eta k_1 = 1.161$ in Theorem 4.2. This implies that when α is used as the bifurcation parameter, the bifurcation direction at $\alpha = \alpha^* = 0.3179$ near the infection-free equilibrium E_0 is forward if $\rho < \bar{\rho} = 1.161$ and the direction is backward if $\rho > \bar{\rho} = 1.161$, which accurately corresponds to the dynamics shown in Fig. 1 ($B_1 = (1.161, 0.3179)$) and Fig. 2.

Next, we explore the bifurcations of the periodic orbits. The Hopf bifurcation points H_{sub} and $\bar{H}_{super}$ in Fig. 2e are used as initial points respectively, and then we continue to draw the bifurcation diagrams of the periodic orbits, which are depicted in Fig. 3a, b. It is observed from Fig. 2e that model (1) generates an unstable periodic orbit as parameter α increases near H_{sub}. Figure 3a further shows that the amplitude of this

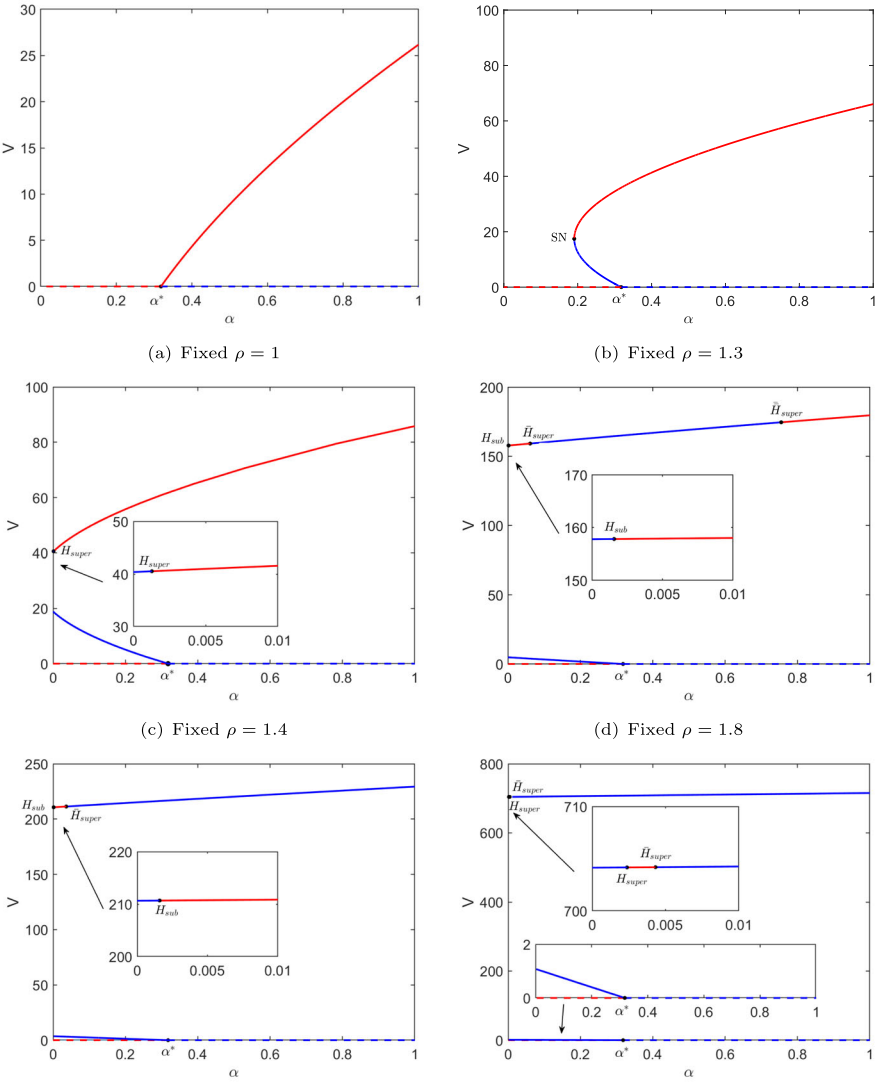

(a) Fixed $\rho = 1$ (b) Fixed $\rho = 1.3$

(c) Fixed $\rho = 1.4$ (d) Fixed $\rho = 1.8$

(e) Fixed $\rho = 2$ (f) Fixed $\rho = 3.9$

Fig. 2 Bifurcation diagrams of component V of equilibria of the model with respect to parameter α for different values of parameter ρ, where $\alpha^* = 0.3179$ corresponding to $\mathcal{R}_0 = 1$. SN(on SNC) corresponds to saddle node bifurcation, H(on HBC_1), $\bar{H}$ and $\bar{\bar{H}}$(on HBC_2) express Hopf bifurcation where the subscripts *super* and *sub* represent that the Hopf bifurcation is supercritical and subcritical, respectively. The dashed and solid curves represent E_0 and E^*, where the red curve expresses stable equilibrium and the blue curve shows unstable one

Table 3 The corresponding thresholds regarding parameter α in Fig. 2

	Threshold	First Lyapunov coefficient
Figure 2b	$\alpha_{SN} = 0.1907$	–
Figure 2c	$\alpha_{H_{super}} = 0.00128$	$-2.930474 \times 10^{-14}$
Figure 2d	$\alpha_{H_{sub}} = 0.001563$	4.520355×10^{-15}
	$\alpha_{\bar{H}_{super}} = 0.06112$	$-3.495590 \times 10^{-11}$
	$\alpha_{\bar{H}_{super}} = 0.7551$	-2.182371×10^{-8}
Figure 2e	$\alpha_{H_{sub}} = 0.001595$	7.722922×10^{-15}
	$\alpha_{\bar{H}_{super}} = 0.03641$	$-1.337931 \times 10^{-11}$
Figure 2f	$\alpha_{H_{super}} = 0.004319$	$-1.290048 \times 10^{-13}$
	$\alpha_{\bar{H}_{super}} = 0.002378$	$-4.973064 \times 10^{-15}$

periodic orbit bifurcated from H_{sub} increases as α increases until it undergoes the saddle node bifurcation at $\alpha = \alpha_{SNC} = 0.001625$. Another stable periodic orbit appears and the amplitude increases as α decreases. Therefore, we choose $\alpha = 0.00162$ to show the dynamics of model (1) in this case. Figure 3c, d show a larger stable periodic orbit (red) and a smaller unstable periodic orbit (blue), that is, the model has a stable infection-free equilibrium $E_0 = (1000, 0, 0, 0)$, a stable infected equilibrium $E_1^* = (42512, 937.66, 687979, 210.68)$, a stable periodic solution and an unstable infected equilibrium $E_2^* = (42512, 15.991, 11732, 3.5929)$ at the same time. They are generated by four different initial values (500, 1500, 500, 50), (30000, 500, 500000, 100), (5000, 500, 410000, 100) and (1300, 1200, 890000, 250), respectively. Figure 2e also shows that model (1) produces a stable periodic orbit as α increases near $\bar{H}_{super}$. Differently, we can see from Fig. 3b that the periodic orbit bifurcated from $\bar{H}_{super}$ undergoes a saddle node bifurcation at $\alpha = \alpha_{H\bar{N}C} = 0.07035$, but another unstable periodic orbit appears when $\alpha = 0.06842$. Therefore, we choose $\alpha = 0.069$ to plot the phase diagram and solution trajectories of model (1), which can be seen in Figure (3)e, d. It is observed from them that model (1) has a larger unstable periodic orbit and a smaller stable periodic orbit, that is, the model has a stable infection-free equilibrium $E_0 = (1000, 0, 0, 0)$, a stable periodic solution and two unstable infected equilibria $E_1^* = (4319.2, 943.54, 65589, 212.00)$ and $E_2^* = (4319.2, 12.506, 869.37, 2.8099)$ at the same time. They are generated by three different initial values (2000, 50, 2000, 50), (2300, 200, 240000, 150) and (11820, 1770, 38600, 350), respectively.

From Figs. 1 and 2, we can observe that parameters α and ρ greatly affect the dynamics of model (1). When ρ is small, if α is also small (region ③), the model (1) only has a unique stable infection-free equilibrium, indicating that the HIV infection will be eradicated. But if α is large (region ①), the model (1) has one stable infected equilibrium and the infection-free equilibrium is unstable, indicating that the infection will persist. When ρ is large, if α is small (region ④ and ⑤), the model has very complex dynamics that makes the infection is unpredictable. If α is large (region ②the

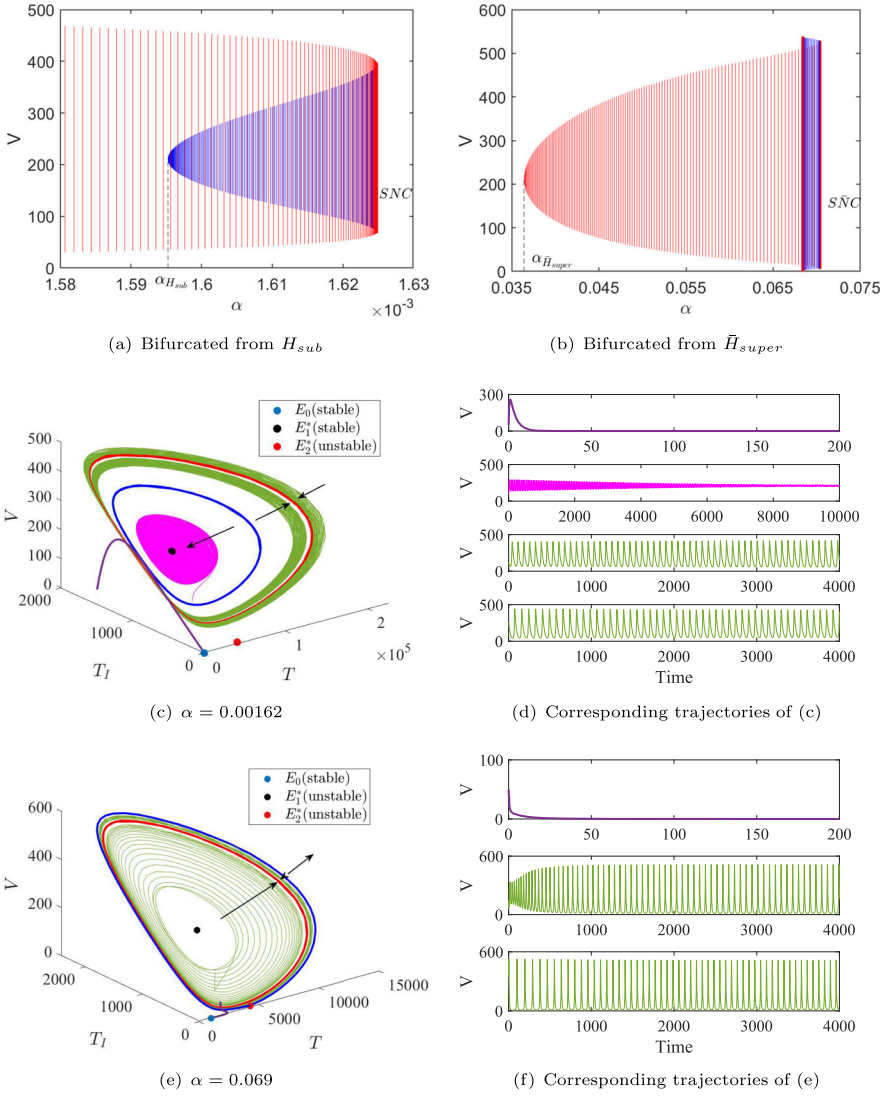

(a) Bifurcated from H_{sub}

(b) Bifurcated from $\bar{H}_{super}$

(c) $\alpha = 0.00162$

(d) Corresponding trajectories of (c)

(e) $\alpha = 0.069$

(f) Corresponding trajectories of (e)

Fig. 3 **a**, **b** Bifurcation diagrams of the periodic orbit generated by the Hopf bifurcation point H_{sub} and $\bar{H}_{super}$ in Fig. 2e. **c–f** are the phase diagrams and solution trajectories of model (1) when $\alpha = 0.00162$ in (**a**) and $\alpha = 0.069$ in (**b**), respectively. The red and blue curves represent stable and unstable periodic orbits respectively

equilibria of the model (1) are unstable, but there exists at least a periodic solution, which will make the infection difficult to be controlled. To sum up, obviously, the smaller the ρ is controlled, the better it is for controlling HIV infection. When ρ is small, α should be controlled to be as small as possible. However, when ρ is large, controlling α alone cannot effectively control HIV infection, and the changes in T cells

are highly dependent on initial conditions. This may provide a new and meaningful perspective for HIV treatment strategies.

6 Model fitting to quantify the effects of cART

6.1 Model fitting and parameters estimation

In clinical practice, there are cases where patients delay initiation of therapy following an HIV diagnosis. However, the timing of treatment is crucial for restoring immune function and achieving rapid virus suppression (Dijkstra et al. 2021). When considering the effects of the cART and the timing of treatment, model (1) is extended into the following model (9) (Herz et al. 1996; Yang and Xiao 2010).

$$\begin{aligned}
\frac{dT}{dt} &= \lambda + \frac{\rho}{\eta + V} TV - \bar{k}_1 TV - d_1 T, \\
\frac{dT_I}{dt} &= \alpha \bar{k}_1 TV + \beta T_L - d_2 T_I, \\
\frac{dT_L}{dt} &= (1-\alpha)\bar{k}_1 TV - \beta T_L - d_3 T_L, \\
\frac{dV}{dt} &= k_2 T_I - d_4 V,
\end{aligned} \tag{9}$$

where

$$\bar{k}_1 = \begin{cases} k_1, & if\, t \leqslant t^*, \\ k_1\,(1-\epsilon)\,, & if\, t > t^*. \end{cases}$$

The reverse transcriptase (RT) inhibitor blocks infection and hence reduces k_1 (Perelson and Nelson 1999; Huang 2010). Parameter ϵ depicts the effectiveness of the RT inhibitor. If $\epsilon = 1$, the inhibition is 100% effective, whereas if $\epsilon = 0$, there is no inhibition. When $t = 0$, the patient is first diagnosed, and $t = t^*$ is the time when treatment begins.

The data used to fit the model comes from 8 adult patients being treated with a three-drug regimen at the Second Hospital of Nanjing. Inclusion criteria were HIV-infected adults aged 18 years or older with available $CD4^+$ T cell count records before and after treatment between January 2008 and December 2022, while exclusion criteria included patients with severe comorbidities, such as cancer or significant liver or kidney dysfunction. The three-drug regimen used by the patients consisted of two nucleoside reverse transcriptase inhibitors (NRTIs) and one non-nucleoside reverse transcriptase inhibitor (NNRTI). Baseline characteristics, such as age, gender, and route of infection, were recorded at the time of treatment. During the course of treatment, $CD4^+$ T cell count was measured once or twice annually, using flow cytometry to ensure data accuracy. The median age of the patients at the time of treatment initiation was 35 years, and the median baseline $CD4^+$ T cell count was 654 cells per μL. The Ethics Committee of the Second Hospital of Nanjing approved the study and waived

the requirement for informed consent. Personal information of study participants was kept strictly confidential, and all information was used only for scientific research. The dynamic model (9) is fitted to $CD4^+$ T cells data from patients by the using least squares method. To compare the best fits with different assumptions, the sum of squared residuals(SSR) is calculated. The estimation of parameters and numerical simulations are conducted by Matlab R2022a. For all patients, we estimate parameter values and calculate the mean and variance of them which are given in Table 4. We find a variation in the estimates of all individual parameters between patients. The coefficients of variation (CV) range from 1.9% to 130.8% for different parameters.

Figure 4 shows the dynamics of the uninfected $CD4^+$ T cell population. There exists a discernible pattern in the change of $CD4^+$ T cell count among patients from pre-treatment to post-treatment. As example, Fig. 4a presents the model fitting results for Patient01. After diagnosis, there is a rapid decrease of $CD4^+$ T cells, followed by a slight recovery. Then the population achieves steady state in the absence of treatment. The simulation is consistent with the typical pattern (Simon and Ho 2003), where $CD4^+$ T cell count drops after infection, climbs to a level after the virus has peaked, and then drops back to the eventual level attained in the asymptomatic stage. Upon starting treatment, $CD4^+$ T cells experience a significant increase. Subsequently, the trend gradually stabilizes, reaching a dynamic equilibrium. The data provide support for the observed finding that robust $CD4^+$ T cell responses to cART could sustain over several years (Nash et al. 2008).

6.2 Sensitivity analysis

Sensitivity analysis is performed to find sensitive parameters influencing the changes in the number of $CD4^+$ T cells and virus load using partial rank correlation coefficients (PRCCs) (Marino et al. 2008). Assuming that the input parameters are normally distributed, the expectations and standard deviations are the estimated values in Table 4. The values of components T and V of the stable infected equilibrium are the output values, respectively. In Table 5, the magnitude of the index determines the sensitivity and the sign of the index represents either a positive or negative correlation. The significance level is chosen as 0.05.

In Fig. 5, PRCCs suggest that λ, ϵ, and d_1 are the most significant parameters for $CD4^+$ T cells. For viral load, the most sensitive parameters are k_2, λ, and d_4. It is observed that drug efficacy ϵ is significantly sensitive to the number of variables T and V. Therefore, we further study how the steady-state of $CD4^+$ T cells and viral load change as drug efficacy increases by using parameters from Patient01. Figure 6a shows that the number of $CD4^+$ T cells in steady state is very sensitive to drug efficacy, particularly when $CD4^+$ T cell count is relatively high as drug efficacy increases. From Fig. 6b it can also be found that there exists a threshold of drug efficacy (ϵ^*) such that $\mathcal{R}_0 = 1$. When $\epsilon \geq \epsilon^*$, the viral load could be completely eliminated in theory.

Table 4 Parameter values of best fits of model (9) to eight treated patients

	1	2	3	4	5	6	7	8	Mean	SD	CV(%)
λ	5	9	13	13	20	10	33	16	15	9	57.8
ρ	0.010	0.067	0.038	0.0018	0.012	0.075	0.051	0.0092	0.033	0.029	86.7
η	570	227	226	300	453	495	284	443	375	132	35.2
β	0.0031	0.0019	0.0024	0.0064	0.00060	0.0015	0.0035	0.0022	0.0027	0.0018	65.3
α	0.98	0.98	0.95	0.93	0.96	0.94	0.93	0.96	0.95	0.018	1.9
k_1	0.000061	0.000074	0.000029	0.000038	0.000053	0.000068	0.00045	0.000086	0.00011	0.00014	130.8
k_2	205.48	381.99	484.36	476.93	102.50	358.21	87.99	514.45	326.49	172.66	52.9
d_1	0.0083	0.011	0.017	0.012	0.010	0.026	0.037	0.027	0.019	0.010	55.7
d_2	0.37	0.70	0.65	1.02	0.42	0.33	0.86	0.73	0.64	0.25	38.7
d_3	0.00013	0.00018	0.00011	0.00054	0.00084	0.00063	0.00073	0.00075	0.00049	0.00030	61.6
d_4	11.38	16.80	10.59	14.93	8.20	11.92	25.24	22.34	15.17	5.98	39.4
$T(0)$	400	552	1467	1538	797	15	543	434	718	531	74.0
$T_I(0)$	270	70	43	35	176	89	351	301	167	126	75.4
$T_L(0)$	382	223	424	468	123	100	412	104	280	158	56.4
$V(0)$	11,147	88,018	3694	53,109	48,224	56,899	52,438	89,795	50,415	31048	61.6
ϵ	0.44	0.84	0.84	0.43	0.76	0.83	0.41	0.73	0.66	0.20	29.9
ϵ^*	0.44	0.48	0.36	0.25	0.67	0.58	0.38	0.36	0.44	0.13	30.4

Note: Parameter units are the same as in Table 1

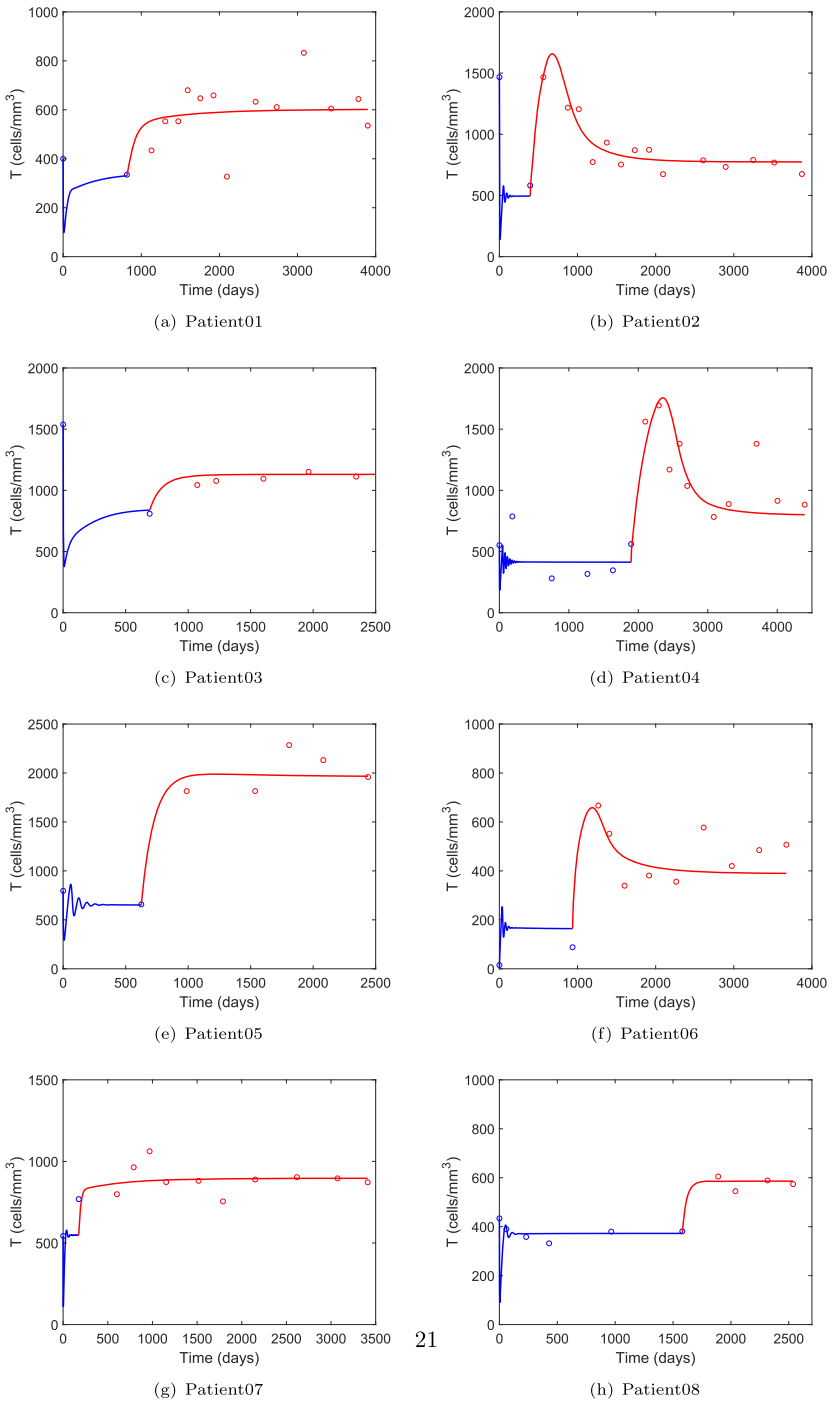

Fig. 4 Dynamics of CD4$^+$ T cells (mm^{-1}) over the days. Simulation results are compared with clinical data. Blue and red points correspond to before and after treatment clinical data, while solid blue and red curves denote fitting results before and after treatment, respectively

Table 5 The PRCCs values on the outcome of components T and V of the stable infected equilibrium respectively

Parameter	PRCC for T	P value	PRCC for V	P value
λ	0.5452	0.0000*	0.4118	0.0000*
ρ	0.0666	0.0000*	0.3116	0.0000*
η	−0.0576	0.0000*	−0.1698	0.0000*
β	0.0225	0.0145	−0.0072	0.4315
α	−0.0186	0.0431	0.0169	0.0663
k_1	−0.3861	0.0000*	0.1739	0.0000*
k_2	−0.3546	0.0000*	0.4268	0.0000*
d_1	−0.4415	0.0000*	−0.3578	0.0000*
d_2	0.3378	0.0000*	−0.3743	0.0000*
d_3	0.0083	0.3683	−0.0347	0.0002*
d_4	0.3322	0.0000*	−0.3817	0.0000*
ϵ	0.4541	0.0000*	−0.2603	0.0000*

The superscript "$*$" represents that the significance P$<$ 0.01
[1] All parameter values are derived from Table 4 (Mean values)

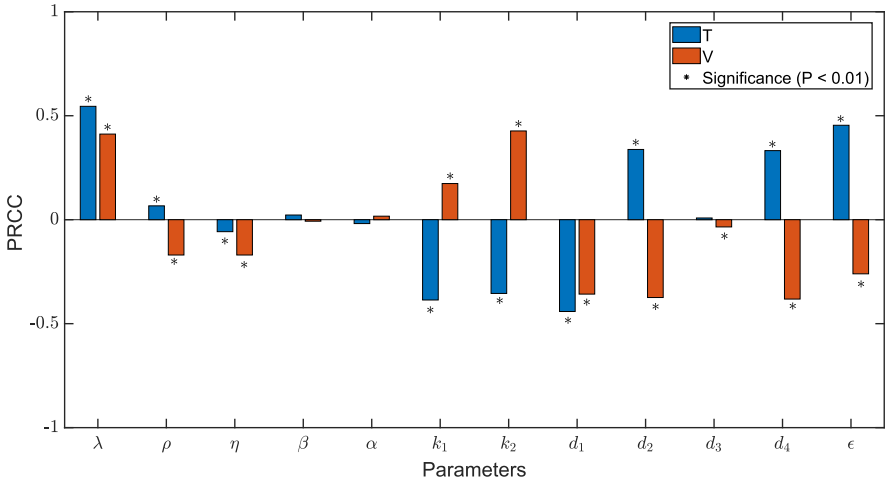

Fig. 5 Sensitivity tests of uninfected CD4$^+$ T cells (T) and viruses (V) to all parameters in model (9). The specific values of PRCCs could be observed from Table 5

6.3 Relation between parameters

We investigate the relationships between parameters using the Spearman rank correlation test. All P values are 2-sided with a significance level of 0.05. We find that the infection rate of uninfected CD4$^+$ T cells by virus (k_1) is significantly positively correlated with the clearance rate of virus particles (d_4); $r = 0.810$, $P = 0.021$. The activate rate of latently infected CD4$^+$ T cells (β) is significantly negatively correlated

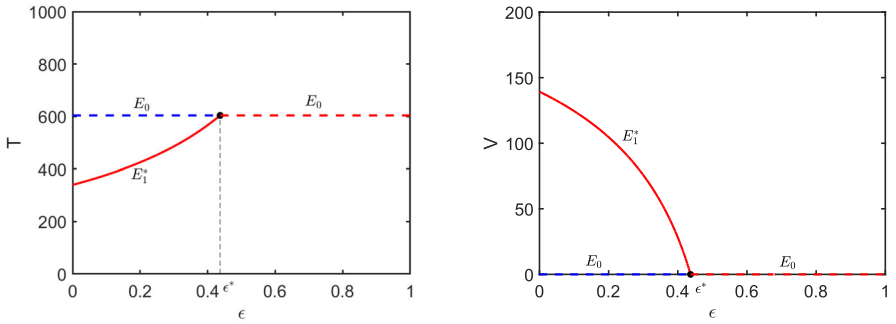

Fig. 6 Bifurcation diagrams of components T and V of the equilibria with respect to parameter ϵ. The threshold value $\epsilon^* = 0.437$ corresponds to $\mathcal{R}_0 = 1$. The dashed and solid curves represent E_0 and E_1^* respectively, where the red curves express the stable equilibrium and the blue curves show the unstable one. Other parameter values are taken from Table 4 (Patient01)

with threshold of drug efficacy (ϵ^*); $r = -0.810$, $P = 0.021$. Other correlations are summarized in Table 6.

7 Conclusion and discussion

In this article, we firstly construct a mathematical model considering HIV latency and the homeostatic proliferation of CD4$^+$ T cells. The dynamics of the model are analyzed in detail. Secondly, we introduce the cART into the model (1), fit the model (9) to clinical data and estimate the parameters. Finally, we perform sensitivity analysis and correlation analysis to investigate the effects of cART and the biological mechanisms of HIV infection and persistence.

For model (1), we discuss the positivity of the solution, calculate $\mathcal{R}_0$ and investigate the existence and stability of equilibria. We theoretically and numerically show that bistability can be caused by a backward bifurcation in presence of HIV latency and the homeostatic proliferation of CD4$^+$ T cells. Our results reveal that if the homeostatic proliferation of CD4$^+$ T cells is insufficient, then backward bifurcation cannot occur. This means that when $\rho < \overline{\rho}$, the infected equilibrium does not exist as long as $\mathcal{R}_0 < 1$, and the virus will be eliminated. However, when $\rho > \overline{\rho}$, two infected equilibria exist even with $\mathcal{R}_0 < 1$. In this case, with a high initial viral load, the larger infected equilibrium tends to be locally asymptotically stable, preventing the virus from being eliminated. This highlights the critical impact of CD4$^+$ T cell homeostatic proliferation on the complete eradication of the virus. We also theoretically prove the existence of Hopf bifurcation at the infected equilibrium. Numerical results show that when ρ is small, α should be minimized to achieve HIV eradication. However, when ρ is large, controlling α alone cannot effectively manage HIV infection, and the changes in CD4$^+$ T cell counts are highly dependent on the initial conditions.

Next, we plot some one-parameter bifurcation diagrams with respect to parameter α when fixing different values of parameter ρ. Saddle node bifurcations, subcritical

Table 6 The Spearman correlation coefficients between the parameters

	λ	ρ	η	β	α	k_1	k_2	d_1	d_2	d_3	d_4	$T(0)$	ϵ	ϵ^*
λ														
ρ	−0.144													
η	−0.252	−0.167												
β	0.036	−0.476	−0.238											
α	−0.599	−0.119	0.286	−0.357										
k_1	0.228	0.310	0.071	−0.048	0.000									
k_2	−0.204	−0.357	−0.333	0.071	0.190	−0.262								
d_1	0.563	0.214	−0.333	0.190	−0.643	0.524	0.167							
d_2	0.479	−0.452	−0.571	0.643	−0.429	0.190	0.238	0.405						
d_3	0.707	−0.095	0.310	−0.381	−0.238	0.452	−0.286	0.310	0.143					
d_4	0.228	0.048	−0.262	0.405	−0.262	0.810^+	0.071	0.667	0.643	0.214				
$T(0)$	0.299	−0.381	−0.643	0.286	−0.286	−0.595	0.238	−0.167	0.571	−0.143	−0.214			
ϵ	−0.359	0.476	−0.310	−0.643	0.357	−0.357	0.405	−0.190	−0.500	−0.357	−0.476	0.071		
ϵ^*	−0.108	0.571	0.476	-0.810^+	0.310	0.238	−0.595	−0.333	−0.690	0.381	−0.310	−0.476	0.262	1.000

The superscript "+" denotes the significance $P < 0.05$

and supercritical Hopf bifurcations can be observed from Fig. 2. We also detect the saddle node bifurcations of the periodic orbits and find the coexistence of the periodic orbits in two cases, one is that the large periodic orbit is stable and the small one is unstable, and the other is the opposite (see Fig. 3). These findings suggest that the homeostatic proliferation of $CD4^+$ T cells and the production of latently infected $CD4^+$ T cells greatly affect the model dynamics, and play a critical role in HIV infection and persistence.

Furthermore, we incorporate cART into the model (1) and fit the modified model (9) to $CD4^+$ T cells data from patients with available records both before and after treatment (Fig. 4). Despite the varying trajectories of $CD4^+$ T cell counts in patients, model (9) provides good fits to the $CD4^+$ T cells data. And the model (9) successfully duplicates the initial decrease and subsequent increase of healthy T cells during early infection before treatment (Clark et al. 1991). Upon starting cART, the parameter ϵ, representing overall drug efficacy, largely explains the recovery of $CD4^+$ T cells. By ensuring consistency of parameters before and after treatment, our model enables to generate a more accurate assessment of the cumulative effect of antiviral therapy. The estimated parameters exhibit similarities with findings from prior research (Hill et al. 2018). Specifically, the values for parameters β (Luo et al. 2012), k_2 (Huang et al. 2006), d_2 (Luo et al. 2012; Huang et al. 2010), d_3 (Hill et al. 2018), and d_4 (Markowitz et al. 2003) are consistent with the previously reported optimal estimates for these variables. Previous studies have estimated the range of drug efficacy to be between 0.67 and 0.88 (Luo et al. 2012) and 0.64 to 0.84 (Putter et al. 2002). However, in this article, the estimated range has shifted lower, from 0.40 to 0.84. One reason for this shift may be that prior studies have predominantly utilized patients data from short-term, precisely controlled clinical trial. In contrast, the data used in this study are derived from real-world settings, where patients have much longer medication cycles and may not adhere to their regimens as strictly as those in clinical trials, resulting in a generally lower overall drug efficacy.

We find that when the effectiveness of the cART approaches a critical threshold, the $CD4^+$ T cells achieve maximum recovery. However, the current drug therapies for HIV-infected patients are not perfect effective. Iwami et al. (2015) investigated the dynamics of cell-to-cell and cell-free HIV-1 infections through experimental-mathematical investigation, suggesting that even a complete block of the cell-free infection would provide only a limited impact on HIV-1 spread. Fortunately, antiviral therapy can still greatly enhance the immune function of patients. Note that if the drug efficacy increases, then both the quantity of $CD4^+$ T cells at steady-state and the rate of $CD4^+$ T cells recovery rise gradually (Fig. 6). This implies that once treatment is initiated, it is highly necessary to enhance the efficacy of drug therapy by improving adherence, monitoring drug resistance and various strategies. Previous studies (Rong et al. 2007; Wang and Rong 2019) have confirmed that as drug efficacy increases, the viral load is suppressed to a lower level.

In addition, correlation analysis shows that the activate rate of latently infected $CD4^+$ T cells (β) is significantly negatively correlated with threshold of drug efficacy (ϵ^*). This suggests that a lower activation rate of latently infected $CD4^+$ T cells in a patient requires a higher threshold of drug efficacy to effectively inhibit viral replication in long-term. This means that the higher the rate at which latently infected

cells transition into actively infected cells, the more beneficial it is for clearing the virus through treatment. Currently, substantial efforts are being directed towards developing a class of drugs called latency-reversing agents (LRAs) that aim to activate HIV gene expression in latently infected cells, with the goal of eliminating the viral reservoir and eventually curing HIV infection. Our findings highlight the importance of the need for latently infected cell activation to optimize therapeutic efficacy. Consistent with previous studies (Archin et al. 2012; Elliott et al. 2014; Ke et al. 2015), it is to be expected that enhancing viral clearance would substantially improve the efficacy of LRAs, as evidenced by the findings presented in this study. Correlation analysis also reveals a significant positive correlation between the infection rate of uninfected $CD4^+$ T cells by the virus and the virus clearance rate, indicating a highly dynamic balance between new cycles of infection and virus clearance.

Our proposed model appears to perform well in capturing the trajectories of $CD4^+$ T cells observed under relatively complex clinical situations. However, some limitations exist for this study. Overall treatment effectiveness could be influenced by multiple factors. Various studies have explored viral dynamics models incorporating clinical factors such as drug adherence (Labbé and Verotta 2006; Huang et al. 2006), time-varying drug efficacy (Wu et al. 2005), drug resistance (Rong et al. 2007) and so on. The model we consider in this paper is a basic model with HIV latency. The homeostatic proliferation of $CD4^+$ T cells is included to consider the variations in the initial $CD4^+$ T cell count or the viral load. Besides, further studies need to be done to incorporate some other factors such as CTL immune response (Liu and Kong 2020; Wang and Li 2021), macrophages (Hadjiandreou et al. 2007; Hernandez-Vargas and Middleton 2013) into the dynamics models.

Acknowledgements We sincerely thank the editor and anonymous reviewers for their valuable comments and suggestions which helped us to improve the manuscript significantly. This work was partially supported by the National Natural Science Foundation of China (Nos. 82320108018, 82073673, 12371488) and self-determined research funds of CCNU from the colleges' basic research and operation of MOE (No. CCNU24JC002).

Data availability The data that support the findings of this study are not openly available due to reasons of sensitivity and are available from the corresponding author upon reasonable request. Data are located in patient data repository of the Second Hospital of Nanjing.

Declarations

Conflict of interest The authors declare that they have no known competing financial interests or personal relationships that could have appeared to influence the work reported in this paper.

References

Archin NM, Liberty AL, Kashuba AD et al (2012) Administration of vorinostat disrupts HIV-1 latency in patients on antiretroviral therapy. Nature 487(7408):482–485. https://doi.org/10.1038/nature11286

Castillo-Chavez C, Song B (2004) Dynamical models of tuberculosis and their applications. Math Biosci Eng 1(2):361–404. https://doi.org/10.3934/mbe.2004.1.361

Catalfamo M, Wilhelm C, Tcheung L et al (2011) CD4 and CD8 T cell immune activation during chronic HIV infection: roles of homeostasis, HIV, type I IFN, and IL-7. J Immunol 186(4):2106–2116. https://doi.org/10.4049/jimmunol.1002000

Chomont N, El-Far M, Ancuta P et al (2009) HIV reservoir size and persistence are driven by T cell survival and homeostatic proliferation. Nat Med 15(8):893–900. https://doi.org/10.1038/nm.1972

Chun TW, Carruth L, Finzi D et al (1997) Quantification of latent tissue reservoirs and total body viral load in HIV-1 infection. Nature 387(6629):183–188. https://doi.org/10.1038/387183a0

Clark SJ, Saag MS, Decker WD et al (1991) High titers of cytopathic virus in plasma of patients with symptomatic primary HIV-1 infection. N Engl J Med 324(14):954–960. https://doi.org/10.1056/NEJM199104043241404

DeJesus EX, Kaufman C (1987) Routh-Hurwitz criterion in the examination of eigenvalues of a system of nonlinear ordinary differential equations. Phys Rev A 35(12):5288–5290. https://doi.org/10.1103/PhysRevA.35.5288

Dhooge A, Govaerts W, Kuznetsov YA (2003) Matcont: a matlab package for numerical bifurcation analysis of ODEs. ACM Trans Math Softw 29(2):141–164. https://doi.org/10.1145/779359.779362

Dijkstra M, van Rooijen MS, Hillebregt MM et al (2021) Decreased time to viral suppression after implementation of targeted testing and immediate initiation of treatment of acute human immunodeficiency virus infection among men who have sex with men in Amsterdam. Clin Infect Dis 72(11):1952–1960. https://doi.org/10.1093/cid/ciaa505

Doekes HM, Fraser C, Lythgoe KA (2017) Effect of the latent reservoir on the evolution of HIV at the within- and between-host levels. PLoS Comput Biol 13(1):e1005228. https://doi.org/10.1371/journal.pcbi.1005228

Dong Y, Ma W (2012) Global properties for a class of latent HIV infection dynamics model with CTL immune response. Int J Wavelets Multiresolut Inf Process 10(5):1250045. https://doi.org/10.1142/S0219691312500452

Elliott JH, Wightman F, Solomon A et al (2014) Activation of HIV transcription with short-course vorinostat in HIV-infected patients on suppressive antiretroviral therapy. PLoS Pathog 10(10):e1004473. https://doi.org/10.1371/journal.ppat.1004473

Finzi D, Hermankova M, Pierson T et al (1997) Identification of a reservoir for HIV-1 in patients on highly active antiretroviral therapy. Science 278(5341):1295–1300. https://doi.org/10.1126/science.278.5341.1295

Finzi D, Blankson J, Siliciano JD et al (1999) Latent infection of CD4+ T cells provides a mechanism for lifelong persistence of HIV-1, even in patients on effective combination therapy. Nat Med 5(5):512–517. https://doi.org/10.1038/8394

Hadjiandreou M, Conejeros R, Vassiliadis VS (2007) Towards a long-term model construction for the dynamic simulation of HIV infection. Math Biosci Eng 4(3):489–504. https://doi.org/10.3934/mbe.2007.4.489

Hernandez-Vargas EA, Middleton RH (2013) Modeling the three stages in HIV infection. J Theor Biol 320:33–40. https://doi.org/10.1016/j.jtbi.2012.11.028

Herz AV, Bonhoeffer S, Anderson RM et al (1996) Viral dynamics in vivo: limitations on estimates of intracellular delay and virus decay. Proc Natl Acad Sci USA 93(14):7247–7251. https://doi.org/10.1073/pnas.93.14.7247

Hill AL, Rosenbloom DIS, Nowak MA et al (2018) Insight into treatment of HIV infection from viral dynamics models. Immunol Rev 285(1):9–25. https://doi.org/10.1111/imr.12698

Huang Y (2010) A Bayesian approach in differential equation dynamic models incorporating clinical factors and covariates. J Appl Stat 37(2):181–199. https://doi.org/10.1080/02664760802578320

Huang Y, Liu D, Wu H (2006) Hierarchical Bayesian methods for estimation of parameters in a longitudinal HIV dynamic system. Biometrics. https://doi.org/10.1111/j.1541-0420.2005.00447.x

Huang Y, Wu H, Acosta EP (2010) Hierarchical bayesian inference for HIV dynamic differential equation models incorporating multiple treatment factors. Biom J 52(4):470–486. https://doi.org/10.1002/bimj.200900173

Iwami S, Takeuchi JS, Nakaoka S, et al (2015) Cell-to-cell infection by HIV contributes over half of virus infection. eLife 4:e08150. https://doi.org/10.7554/eLife.08150
Ke R, Lewin SR, Elliott JH et al (2015) Modeling the effects of vorinostat in vivo reveals both transient and delayed HIV transcriptional activation and minimal killing of latently infected cells. PLoS Pathog 11(10):e1005237. https://doi.org/10.1371/journal.ppat.1005237
Kim H, Perelson AS (2006) Viral and latent reservoir persistence in HIV-1-infected patients on therapy. PLoS Comput Biol 2(10):e135. https://doi.org/10.1371/journal.pcbi.0020135
Labbé L, Verotta D (2006) A non-linear mixed effect dynamic model incorporating prior exposure and adherence to treatment to describe long-term therapy outcome in HIV-patients. J Pharmacokinet Phar 33(4):519–542. https://doi.org/10.1007/s10928-006-9022-4
Liu C, Kong L (2020) Dynamics of an HIV model with cytotoxic T-lymphocyte memory. Adv Differ Equ 1:581. https://doi.org/10.1186/s13662-020-03035-8
Loudon T, Pankavich S (2017) Mathematical analysis and dynamic active subspaces for a long term model of HIV. Math Biosci Eng 14(3):709–733. https://doi.org/10.3934/mbe.2017040
Luo R, Piovoso MJ, Martinez-Picado J et al (2012) HIV model parameter estimates from interruption trial data including drug efficacy and reservoir dynamics. PLoS ONE 7(7):e40198. https://doi.org/10.1371/journal.pone.0040198
Marino S, Hogue IB, Ray CJ et al (2008) A methodology for performing global uncertainty and sensitivity analysis in systems biology. J Theor Biol 254(1):178–196. https://doi.org/10.1016/j.jtbi.2008.04.011
Markowitz M, Louie M, Hurley A et al (2003) A novel antiviral intervention results in more accurate assessment of human immunodeficiency virus type 1 replication dynamics and T-cell decay in vivo. J Virol 77(8):5037–5038. https://doi.org/10.1128/jvi.77.8.5037-5038.2003
Marsden JE, McCracken M (1976) The Hopf bifurcation and its applications. Springer, New York. https://doi.org/10.1007/978-1-4612-6374-6
Moreno-Fernandez ME, Presicce P, Chougnet CA (2012) Homeostasis and function of regulatory T cells in HIV/SIV infection. J Virol 86(19):10262–10269. https://doi.org/10.1128/JVI.00993-12
Mzingwane ML, Tiemessen CT (2017) Mechanisms of HIV persistence in HIV reservoirs. Rev Med Virol. https://doi.org/10.1002/rmv.1924
Nash D, Katyal M, Brinkhof MWG et al (2008) Long-term immunologic response to antiretroviral therapy in low-income countries: a collaborative analysis of prospective studies. AIDS 22(17):2291–2302. https://doi.org/10.1097/QAD.0b013e3283121ca9
Pankavich S, Neri N, Shutt D (2020) Bistable dynamics and Hopf bifurcation in a refined model of early stage HIV infection. Discrete Contin Dyn Syst Ser B 25(8):2867–2893. https://doi.org/10.3934/dcdsb.2020044
Perelson AS, Nelson PW (1999) Mathematical analysis of HIV-1 dynamics in vivo. SIAM Rev 41(1):3–44. https://doi.org/10.1137/S0036144598335107
Perelson AS, Kirschner DE, De Boer R (1993) Dynamics of HIV infection of CD4+ T cells. Math Biosci 114(1):81–125. https://doi.org/10.1016/0025-5564(93)90043-a
Perelson AS, Essunger P, Cao Y et al (1997) Decay characteristics of HIV-1-infected compartments during combination therapy. Nature 387(6629):188–191. https://doi.org/10.1038/387188a0
Putter H, Heisterkamp SH, Lange JMA et al (2002) A Bayesian approach to parameter estimation in HIV dynamical models. Stat Med 21(15):2199–2214. https://doi.org/10.1002/sim.1211
Reeves DB, Duke ER, Wagner TA et al (2018) A majority of HIV persistence during antiretroviral therapy is due to infected cell proliferation. Nat Commun 9(1):4811. https://doi.org/10.1038/s41467-018-06843-5
Rong L, Feng Z, Perelson AS (2007) Emergence of HIV-1 drug resistance during antiretroviral treatment. Bull Math Biol 69(6):2027–2060. https://doi.org/10.1007/s11538-007-9203-3
Rong SY, Guo T, Smith JT et al (2023) The role of cell-to-cell transmission in HIV infection: insights from a mathematical modeling approach. Math Biosci Eng 20(7):12093–12117. https://doi.org/10.3934/mbe.2023538
Shu H, Wang L (2012) Role of CD4 + T-cell proliferation in HIV infection under antiretroviral therapy. J Math Anal Appl 394(2):529–544. https://doi.org/10.1016/j.jmaa.2012.05.027
Siliciano JD, Kajdas J, Finzi D et al (2003) Long-term follow-up studies confirm the stability of the latent reservoir for HIV-1 in resting CD4+ T cells. Nat Med 9(6):727–728. https://doi.org/10.1038/nm880
Simon V, Ho DD (2003) HIV-1 dynamics in vivo: implications for therapy. Nat Rev Microbiol 1(3):181–190. https://doi.org/10.1038/nrmicro772

UNAIDS (2023) The path that ends AIDS: UNAIDS global AIDS update 2023. https://www.unaids.org/sites/default/files/media_asset/2023-unaids-global-aids-update_en.pdf/ (accessed 23 May 2024)
Van den Driessche P, Watmough J (2002) Reproduction numbers and sub-threshold endemic equilibria for compartmental models of disease transmission. Math Biosci 180(1):29–48. https://doi.org/10.1016/S0025-5564(02)00108-6
Wang A, Li MY (2021) Viral dynamics of HIV-1 with CTL immune response. Discrete Contin Dyn Syst Ser B 26(4):2257–2272. https://doi.org/10.3934/dcdsb.2020212
Wang S, Wang S (2024) Delayed nonmonotonic immune response in HIV infection system. Math Methods Appl Sci 47(7):6683–6714. https://doi.org/10.1002/mma.9945
Wang S, Wang T, Xu F et al (2024) Bistability of an HIV model with immune impairment. SIAM J Appl Dyn Syst 23(2):1108–1132. https://doi.org/10.1137/23M1596004
Wang X, Rong L (2019) HIV low viral load persistence under treatment: insights from a model of cell-to-cell viral transmission. Appl Math Lett 94:44–51. https://doi.org/10.1016/j.aml.2019.02.019
Wang X, Mink G, Lin D et al (2017) Influence of raltegravir intensification on viral load and 2-LTR dynamics in HIV patients on suppressive antiretroviral therapy. J Theor Biol 416:16–27. https://doi.org/10.1016/j.jtbi.2016.12.015
Wu H, Huang Y, Acosta EP et al (2005) Modeling long-term HIV dynamics and antiretroviral response: effects of drug potency, pharmacokinetics, adherence, and drug resistance. J Acquir Immune Defic Syndr 39(3):272–283. https://doi.org/10.1097/01.qai.0000165907.04710.da
Yang Y, Xiao Y (2010) Threshold dynamics for an HIV model in periodic environments. J Math Anal Appl 361(1):59–68. https://doi.org/10.1016/j.jmaa.2009.09.012
Zhang J, Takeuchi Y, Dong Y et al (2024) Modelling the preventive treatment under media impact on tuberculosis: a comparison in four regions of China. Infect Dis Model 9(2):483–500. https://doi.org/10.1016/j.idm.2024.02.006

Authors and Affiliations

Jing Cai[1] · Jun Zhang[2] · Kai Wang[3] · Zhixiang Dai[1] · Zhiliang Hu[4] · Yueping Dong[2] · Zhihang Peng[1,5,6]

✉ Yueping Dong
ypdong@ccnu.edu.cn

✉ Zhihang Peng
zhihangpeng@njmu.edu.cn

Jing Cai
caijing@stu.njmu.edu.cn

Jun Zhang
zhj@mails.ccnu.edu.cn

Kai Wang
15651977659@163.com

Zhixiang Dai
zhixiangdai@stu.njmu.edu.cn

Zhiliang Hu
huzhiliangseu@163.com

[1] School of Public Health, Nanjing Medical University, 101 Longmian Road, Nanjing 211166, Jiangsu, China

2 School of Mathematics and Statistics, and Key Laboratory of Nonlinear Analysis and Applications (Ministry of Education), Central China Normal University, 152 Luoyu Road, Wuhan 430079, Hubei, China

3 Department of Pulmonary and Critical Care Medicine, China-Japan Friendship Hospital, No. 2 East Cherry Garden Street, Beijing 100029, China

4 Nanjing Infectious Disease Center, The Second Hospital of Nanjing, Tangshan Street, Nanjing 211113, Jiangsu, China

5 National Key Laboratory of Intelligent Tracking and Forecasting for Infectious Diseases, Chinese Center for Disease Control and Prevention, 155 Changbai Road, Beijing 102206, China

6 National Institute for Viral Disease Control and Prevention, Chinese Center for Disease Control and Prevention, 155 Changbai Road, Beijing 102206, China